

110th Anniversary: Nucleation of Ag nanoparticles in helical microfluidic reactor. Comparison between microwave and conventional heating.

Roberta Manno^{†, ‡, ‡‡}, Victor Sebastian^{(*)†, ‡, ‡‡}, Reyes Mallada^{(*)†, ‡, ‡‡}, Jesús Santamaria^{†, ‡, ‡‡}

† Nanoscience Institute of Aragon and Chemical and Environmental Engineering Department, University of Zaragoza, 50018 Zaragoza, Spain

‡ Networking Research Center CIBER-BBN, 28029 Madrid, Spain

‡‡ Aragón Materials Science Institute, ICMA, CSIC – University of Zaragoza, Pedro Cerbuna 12, 50009 Zaragoza, Spain

ABSTRACT: The synthesis of silver nanoparticles with small average size and narrow size distribution is a requirement for applications in different fields such as antibacterial or catalysis. Previous studies of nanoparticles synthesis confirm the advantages of combining continuous flow and microwave dielectric heating, given the possibilities that arise regarding control of residence time and localized volumetric heating. In this paper, we present two experimental set-ups to perform the continuous synthesis of silver nanoparticles using microwave heating (MWH) and conventional heating (CH). Experimental and simulated data confirm a different temperature profile along the reactor, being more favorable in the case of MWH. As a result, the nanoparticles synthesized under MWH presented a synthesis yield of 54% and a narrow particle size distribution ($19\pm 4.3\text{nm}$). Furthermore, MWH led to reduced wall fouling by deposition of product material and allowed fast cooling of the product stream, preventing further growth of the nanoparticles.

1. INTRODUCTION

Firstly introduced in the early 1990s, microfluidic reactors represent an excellent alternative to batch reactor synthesis. The shift from batch to continuous flow requires a detailed optimization of reactor geometry, residence time, temperature profile, reagent concentration and contact/mixing mode. The reagents are injected by mechanical (low flow pumps such as syringe, HPLC or peristaltic pumps are commonly used), electrostatic or magnetic forces into channels, whose diameters range from 50 to 1000 μm , allowing a precise control of residence time. On the other hand, the small diameter of the reactor channels and low flow rates employed generally result in laminar flow, limiting the mixing. For this reason, intersecting, zigzag, 3D serpentine, twisted or helical channels are adopted as passive mixers^{1 2 3}. Finally, continuous production can be scaled up simply by working with parallel systems. The high flexibility and high control of residence time afforded by these microfluidic reactors makes them especially suitable for nanomaterials synthesis, and thus they have been used for the fabrication of several nanostructures, such as monodisperse monometallic and bimetallic nanoparticles^{4 5}, nanocubes, nanorods, nanosheet, core-shell, Janus structures, dumbbells, etc.^{6 7 8 9 10} The result is usually a reduction of reagents waste, time and temperature and improvement of size distribution and synthesis yield.^{8 11} Unfortunately, microchannel obstruction by deposited nanoparticles still represents a serious challenge for the synthesis of nanomaterials in continuous flow.¹²

Microwave heating (MWH) can be very selective and may involve different mechanisms depending on the materials concerned. For liquid phase, MWH is generally based on the capacity to polarize molecules depending on their dielectric properties. The ability of a material to be heated in the presence of the MWH field is defined by its dielectric loss tangent: $\tan\delta = \epsilon''/\epsilon'$. The dielectric constant (ϵ') determines the electric energy storage in the dielectric, while the dielectric loss factor (ϵ'') measures the dissipation of electric energy in form of heat within the material¹³. The different materials can be divided into three groups regarding their interaction with microwaves: i) Microwave reflectors, e.g. metals ii) Microwave transmitters – materials that are essentially transparent to microwave radiations, e.g. fused quartz, ceramics, zirconia, etc.; $\tan\delta < 0.1$ iii) Microwave absorbers, those able to take up energy from the microwave field and heat rapidly; $\tan\delta > 0.1$ ¹⁴. The synthesis of metallic nanoparticles in batch conditions, under microwave heating, was studied more than a decade ago by Tsuji et al.¹⁵, who demonstrated that varying reagents and reaction temperature could result in a wide range of shape and size for different metallic nanoparticles. In particular, the authors suggested that microwaves promote the formation of hot spots on the surface of aprotic

polar molecules, like PVP, which remarkably accelerate the formation of metallic nanoparticles. Moreover, polar solvents, characterized by high values of dielectric loss, can convert EM energy into thermal energy very fast. The localized rapid rise of temperature enhances product yield, decreasing the reaction time required to produce nanomaterials with similar quality^{16 17}. Another important factor in MWH is the penetration depth of microwaves in the heated medium, defined as the distance in which the intensity of the radiation falls to 1/e of its original value. This penetration depth is very low in the case of polar solvents. As an example, the penetration depth in water at 50°C and 90°C is 3.1 and 5.4 cm respectively¹⁸. This could limit the application of microwaves in batch reactors with high volumes. To overcome this problem, the combination of microwaves and continuous flow reactors represents a winner alternative to traditional techniques^{19 20 17 21}. Furthermore, if the flowing medium is absorbent and the external wall is microwave transparent, the maximum temperature appears in the center of the channel, reducing wall deposition^{20 22}.

The antibacterial capabilities of silver materials have been known for a long time, starting from Roman times when silver coins were dropped into wells to preserve water, to the beginning of the 20th century when the colloidal silver solutions were commercialized as pharmaceuticals. Today it is known that the release of Ag⁺ ions is responsible for the observed antibacterial effects.⁵ Since oxidation of silver materials in a solution is a surface process, the rate of release of Ag⁺ ions increases as particle size is reduced and thus nanomaterials are commonly used to obtain an intense release. However, given the influence of particle size in the release of Ag⁺ ions, it is key to achieve an accurate control of particle size distribution to obtain an efficient tuning of dose and release rate of Ag⁺ for the antibacterial action while at the same time avoiding the excess of Ag that could lead to the so-called argyria illness because of overexposure to silver. Among the methods for the synthesis of silver nanoparticles, polyol-based procedures have been intensely studied. Commonly ethylene glycol is used as solvent and reducing agent of silver nitrate, (or other silver salts) and polyvinylpyrrolidone PVP acts as stabilizing agent of the formed nanoparticles. The synthesis comprises two steps an initial nucleation induction period followed by growth of the existing nucleus, leading to silver crystalline nanoparticles up to 200nm. When carrying out this synthesis in a conventionally heated reactor it is difficult to obtain a homogeneous temperature because of the high-viscosity medium that presents a high heat transfer resistance. Therefore, MWH due to its volumetric heating capacity represents an ideal alternative to obtain faster and more homogeneous heating.

This synthesis has been previously reported under MWH in a batch reactor^{5 23} observing in all the cases high conversion at low reaction times due to the faster heating.

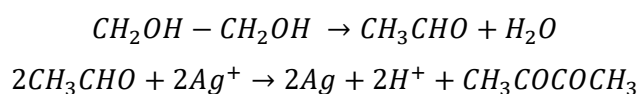
More interestingly, the kinetics of the formation of Ag nanoparticles, under MWH were evaluated by integrating a commercial monomode MWH oven, working at 130 to 160°C, with in situ X-ray diffraction at high energy synchrotron beamline ²⁴. The X-ray started to detect silver nanoparticles after 11 minutes with a size of tenths of nanometers and the final size of the nanoparticles was around 100nm. These kinetic data were further analyzed and reinterpreted by Ozkar and Finke ²⁵ with the conventional mechanism adopted for conventional heating (CH), that considers two successive steps: slow continuous nucleation, first-order reaction (rate constant k_1), followed by a fast autocatalytic surface growth (rate constant k_2). There was some uncertainty in the evaluation of k_1 because the X-ray diffraction technique was not able to detect the initial small clusters of Ag^0 . Nishioka et al. ²³ demonstrated the advantages of combining microwaves and flow chemistry in the polyol method by working at residence times between 2.8 and 28.3s and a nominal temperature of 160°C. The particles synthesized presented a narrow size distribution and the deposition of the internal wall of the reactor drastically decreased. The faster reaction observed with MWH is usually related to the different temperature profile induced. Although the cylindrical monomode cavity employed presented a uniform distribution of the electromagnetic field, the temperature profile observed with a thermographic sensor along the length of the reactor varied from 80 to 160°C. Dzido et al. ²⁶ also reported a continuous synthesis method under MWH observing, in this case, a bimodal size distribution of nanoparticles attributed to the non-isothermal nature of the realized continuous flow process.

The goal of this study is to synthesize in continuous flow silver nanoparticles of a controlled size, i.e. with a narrow size distribution, working at low temperature, in the range (82.7-92.7)°C and low residence time (9 to 54s). Our working hypothesis is that, by achieving a homogeneous distribution of electromagnetic field in a monomode cavity, the temperature distribution in a helical microfluidic reactor can be controlled, allowing to tune nucleation and growth rates. This study also aims to compare MWH against CH in the continuous flow microreactor, using systems that otherwise present the same characteristics concerning reactor design, residence time and reagents. In both systems Ag nanoparticles have been synthesized and characterized at the different flow rates, comparing size distribution, synthesis yield, and wall deposition. To understand the differences observed, a detailed experimental measurement of the temperature, using thermographic camera in the MW heated microreactor and simulation of the temperature profile in the CH microreactor is presented for the first time.

2. EXPERIMENTAL SYSTEM

Synthesis of silver nanoparticles

Silver Nitrate (Aldrich 99.9999%), acted as precursor of silver nanoparticles and was mixed under mechanical stirring, at room temperature, with deionized water (0.157g into 10ml). Polyvinylpyrrolidone (PVP-Sigma Aldrich MWH 55.000) acted as a stabilizer, reducing the agglomeration of the nanoparticles. PVP was mixed under mechanical stirring at 353K with ethylene glycol (Aldrich 99.9%) (2.4g into 10ml). Ethylene glycol (Sigma Aldrich 99.8%) worked as the reducing agent and as the reaction solvent. The reaction occurred according to the following steps ²⁷



The silver nitrate and PVP solutions were pumped through two separated syringes using a high precision syringe pumps (PHD ULTRA by Harvard Apparatus), mixed in a Y-mixer and fed to the reactor. The two inlets presented the same flow rate (range 0.1-0.6 ml/min). The continuous synthesis of Ag NPs was performed in polytetrafluoroethylene (Teflon, Iberfluid Instruments) helical tubular reactors with inner diameter of 0.3875mm and outer diameter of 1.5875 mm. All the Peek connections adopted (ferrules, nuts, luer adapter and Y-mixers) have been provided by IDEX. In detailed, the Y-mixer presents a thru-hole of 0.02'' and a swept volume of 1.7µl. The Teflon pipe was rolled on top of a quartz tube (OD 9mm) and Teflon tape was used to precisely fixed the helix's diameter, pitch distance and the number of turns. The total length of the Teflon tube was 77 cm, which corresponds to 27 turns of the helix and a total reactor volume of 91µl. A schematic representation of the set-up adopted, that could be either heated by MWH or by CH in an oil bath is presented in Figure 1. After synthesis, the samples were centrifuged at 21000 rpm for 15 minutes and washed with acetone to purify them.

The synthesis of nanoparticles in this work has been performed at the facilities of the ICTS "NANBIOSIS" managed by the Nanoparticle Synthesis Unit of CIBER-BBN).

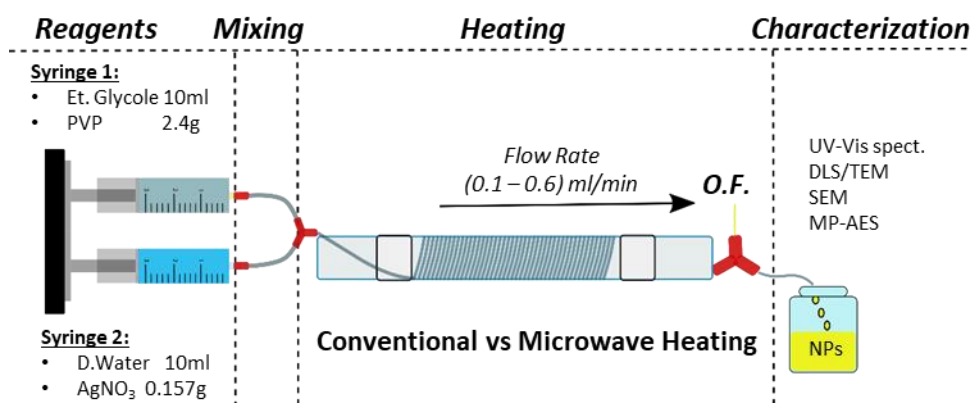


Figure 1 Schematic representation of the experimental set-up for synthesis of silver nanoparticles in microfluidic system. Reaction parameters and heating source (conventional heating or microwaves) are also indicated. An optical fiber (O.F.) was adopted to determine the outlet temperature.

Microwave and conventionally heated systems and temperature measurements

The microwave system, previously described²⁸ was provided by Sairem Iberica and consisted of a solid-state microwave generator operating at 2.43-2.47 GHz with a maximum working power of 150W, a TE10 monomode microwave cavity with a WR340 waveguide and a stub tuner. The microwave field distribution was homogeneous in the central part of the cavity which helped to achieve homogeneous heating, as shown previously with simulation and experimental results²⁹. The power was supplied continuously. A Vector Network Analyzer was adopted to optimize the position of the three stub tuners minimizing the S11 parameter. During synthesis constant values of power and frequency, 20W and 2.45GHz, respectively were applied.

For MWH experiments the reactor was located vertically in the microwave rectangular cavity, the reagents flowed downwards. A commercial T-fitting was modified to locate a Neoptix Optical Fiber sensor (range 193-523 K, Ø: 1mm, marked as O.F. in figures 1 and 2) to measure the temperature of the liquid near the exit of the PTFE tubing. The temperature was measured in two points (Figure 2): O.F.1, which corresponds to the last turn of the helix, and O.F.2, located immediately outside of the cavity at around 47 mm of the last turn. Moreover, a thermographic camera (Optris PI-400038T900) recorded the temperature distribution on the outside surface of PTFE tubing.

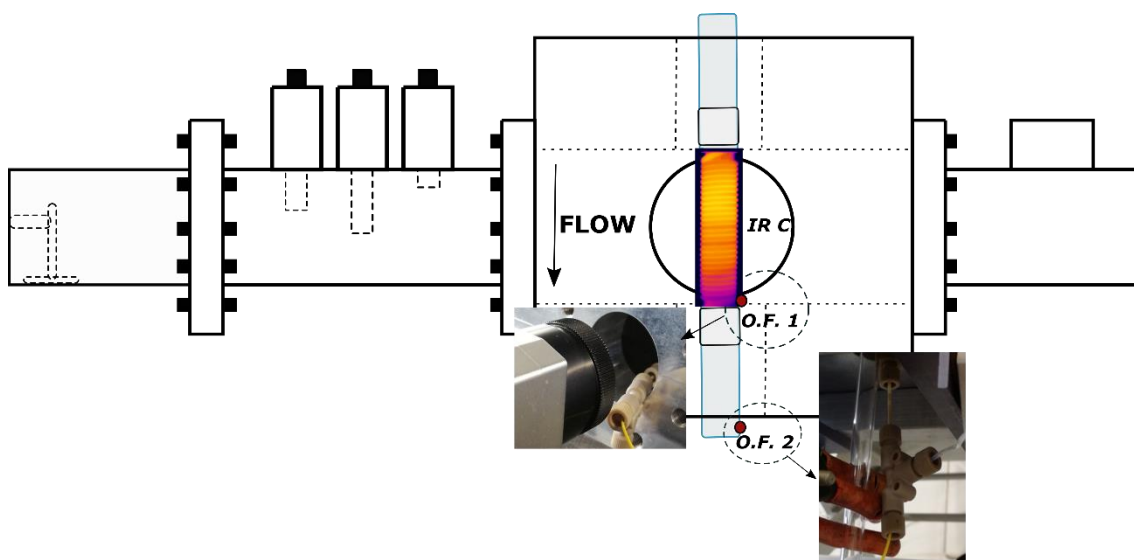


Figure 2 Representation of the rectangular microwave cavity and the location of the reactor. The IR Camera recorded a thermograph of the reactor and the optical fiber measured the temperature in two points: O.F.1 inside the cavity and O.F.2 for the outlet temperature.

In CH experiments, the microfluidic reactor was immersed in a thermostatic bath. The temperature was measured experimentally using an O.F. at four different points inside the tubing corresponding to the end of the 5th, 10th, 20th and 25th turn. In this case, it was not possible to measure the temperature distribution along the reactor immersed in the bath with the thermographic camera. However, we could simulate the temperature profile along the reactor, solving the energy balance at steady state, and the momentum equation, assuming laminar flow (see details about the set of equations used in the supplementary information). The temperature at the inlet of the reactor was 25°C and we assumed that the temperature of the inner wall of the tube was the same as the external bath temperature. The heat evolved during reaction was neglected, given the limited number of moles reacted and the high specific heat of the liquid stream. The heat transfer coefficient, h , was calculated according to the expression developed by Prasad et al.³⁰ for helical tubes in heat exchangers. The software COMSOL Multiphysics simulated the temperature profile by solving the energy balance in the coil reactor. The calculations of the heat transfer coefficient and the parameters entered in the model are presented in the supplementary information. The model was validated by comparing the simulated and experimental temperatures at the 4 experimental measurement points.

Characterization of silver nanoparticles

The synthesized silver NPs were observed by Transmission Electron Microscopy (TEM) in a FEI TECNAI T20 microscope with a maximum energy of 200 keV. A 10 μ L

suspension of the NPs was pipetted onto a TEM copper grid having a continuous carbon film. After complete evaporation, the sample was analyzed by TEM. Particle size distribution of the synthesized nanoparticles was obtained by analysis of at least 120 nanoparticles. Scanning electron microscope (SEM, HITACHI S2300) was employed for the examination of the internal surface of the Teflon pipe. These two microscopes belong to the Laboratory of Advanced Microscopies, LMA, in the installations at the Institute of Nanoscience of Aragon (INA), University of Zaragoza.

Dynamic Light Scattering (Zeta Plus; Brookhaven Instruments Corporation, NY, USA) was performed of each sample after appropriate dilution in Milli-Q-water and sonication of the sample for 5 minutes. At least five replicate measurements were recorded in each case.

UV-Vis Spectroscopy (Agilent 8453 UV-Visible spectrophotometer) was employed to measure surface plasmon resonance SPR of silver nanoparticles, which is a qualitative measure of size distribution and synthesis yield of silver nanoparticles. The spectrophotometric test was performed diluting 100 μ l of sample into 1500 μ l of ethylene glycol and 1500 μ l of distilled water.

The Silver content of liquid samples and suspensions was determined by Microwave Plasma – Atomic Emission Spectroscopy (MP-AES) (Agilent 4100 MP-AES). 3ml of NPs produced sample were centrifuged into 20ml of pure Acetone at 21000rpm for 30 minutes. Supernatant and pellet were analyzed by MP-AES:

-Supernatant: 100 μ l of the supernatant was digested into 2ml with the addition of nitric acid (HNO₃) and hydrochloric acid (HCl) in a volume ratio of 1:3. The resultant digested sample was diluted with Milli-Q water to a final volume of 10 mL for the MP-AES analysis.

-Pellet: The pellet was dispersed in Milli-Q water to a final volume of 10 mL for the analysis. 100 μ l of the sample was digested into 2ml with the addition of nitric acid (HNO₃) and hydrochloric acid (HCl) in a volume ratio of 1:3. The resultant digested sample was diluted with Milli-Q water to a final volume of 10 mL for the MP-AES analysis.

All the characterization experiments presented were repeated at least with three different independent experiments, and average results are presented in the following section.

3. RESULTS AND DISCUSSION

Synthesis of silver nanoparticles under microwave and conventional heating

A preliminary analysis determined the average temperatures under MWH at different flow rates, with a constant power of 20W, using the IR camera to record the temperature profile. Figure 3a) shows an example of the thermographic images employed to determine the average temperature of the external wall of the reactor, T_w . We calculated the average temperature of each turn with the IR image and then average all the turns, resulting in T_w average values (Figure 3b and Table 1) with a relative standard deviation between 4.5 to 10.5%. This deviation is due to the electromagnetic field distribution in the cavity²⁹. If we consider just the 10 central turns, (28 cm), the relative standard deviation of the temperature is lower than 2%. As expected, an increase in the flow rate produces a decrease in the average temperature, the minimum working temperature was 82.7°C. The average temperatures calculated were selected as set point temperatures for the oil bath during CH experiments (see $T_{oil\ bath}$ in Table 1). In this way, the outer surface temperature of the reactor presented the same average temperature for the two modes of heating. Table 1 summarizes all the experiments carried out, indicating the heating source, the flow rate \dot{V} , the residence time t_{res} , and temperature, together with a photograph of the resulting solution after synthesis. It can readily be seen that the solution containing the nanoparticles synthesized with MWs present a more intense color, compared to CH, which may indicate a higher concentration of Ag nanoparticles with bigger dimension.³¹

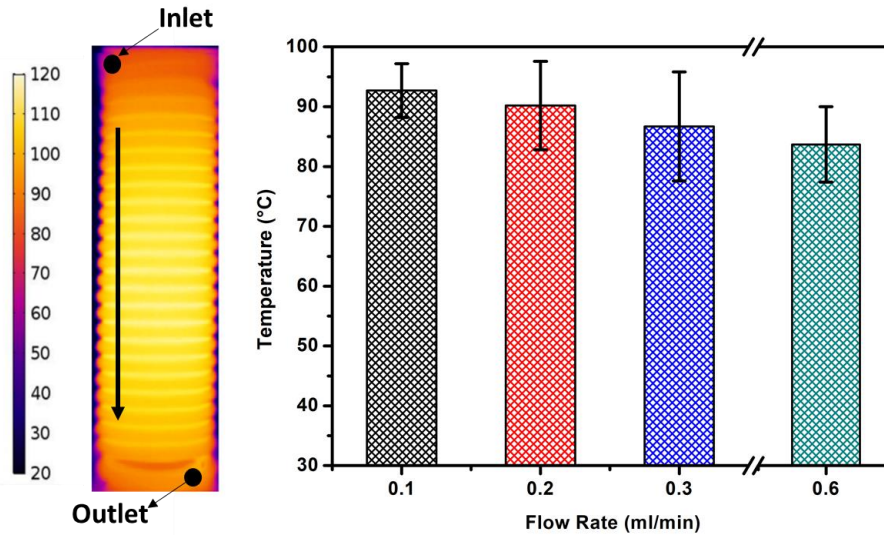
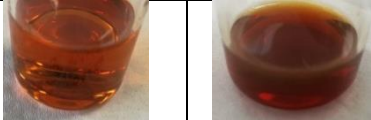





Figure 3 a) Image of thermographic camera showing the outer reactor wall. Temperature readings were used to determine average surface temperatures under microwave heating for different flow rates. b) Average IR temperature obtained under MWH for different flow rates, $P_{MWs}=20W$, $f=2.45GHz$.

Table 1: Summary of experiments and experimental conditions.

Heating Source	\dot{V}	t_{res}	$T_{oil\ bath}$	T_w
CH	MWs	ml/min	°C	°C

	0.1	54	92.7	(92.7±4.5)
	0.2	27	90.2	(90.2±7.4)
	0.3	18	86.7	(86.7±9.1)
	0.6	9	82.7	(82.7±6.3)

The analysis of the UV-Vis spectra, in Figure 4, showed a typical absorption at around 419nm associated with the surface plasmon resonance SPR absorption by silver nanoparticles. The absorption peak intensity decreased for CH and for higher flow rates, i.e. lower residence times. A similar trend was reported by Nishioka et al.²³, at 160°C outlet reaction temperature, where the intensity of the SPR peak decreased from around 0.8 to 0.5 as the residence time decreased from 28 to 2.8s. The absorbance was nearly zero for a residence time of 0.5s. Several factors may affect the differences reported on the absorbance spectra, mainly connected with alterations in the morphology of the nanoparticles and their concentration. The broad shape observed may indicate the presence of a wide distribution of silver nanoparticles in accordance with Mie theory³². This phenomena is especially relevant in Ag nanoparticles produced under a residence time of 54 s, where the bandwidth of MWH produced nanoparticles is larger than the CH ones. According to Mie theory, the bandwidth of silver nanoparticles is very sensitive to particle radius in the range of 1.5-10 nm and 20-40 nm³³. This is in agreement with the particle size histograms reported in figure 5 where it can be observed that mean size of Ag nanoparticles produced by MWH at 54 s residence time are in the size range of 19±4.3 nm, whereas the ones produced by CH are in the range of 10.8±4.7 nm. In any case, the SPR absorption is always more intense under MWH which may indicate a faster conversion of the reaction. This is due to the volumetric heating achieved under microwaves: a fast heating of the inner fluid occurs, resulting in faster nucleation and growth. MP-AES, TEM and DLS analysis were adopted to further investigate the influence of residence time and heating mechanism on the synthesis mechanism. The MP-AES analysis confirmed an increase of synthesis yield of around 13%, (from 41% to 54%) when comparing MWH and CH, for the highest residence time of 54s. This value agrees well with the 42% reported by Grzegorz Dzido²⁶ working at 90°C outlet

temperature of the MWH reactor and a residence time of 12s. These authors observed full conversion only when the reaction temperature was higher than 150°C.

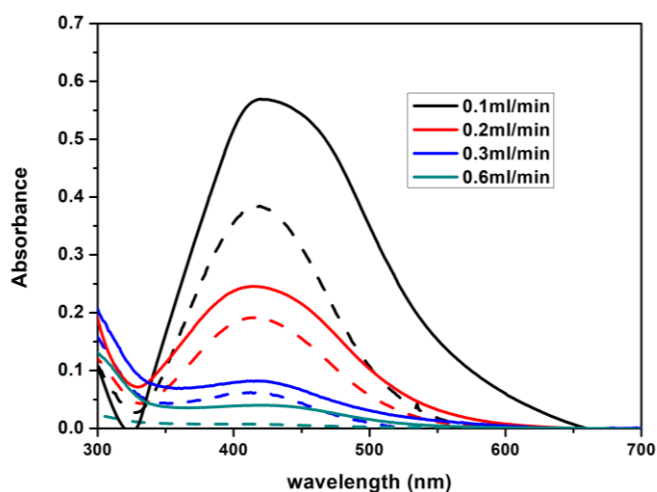


Figure 4 UV-Vis spectra analysis of Ag NPs synthesized at different flow rates. Continuous and dashed lines represent MWs CH, respectively.

TEM and DLS analysis allowed us to determine the particle size distribution of the different experiments. The polydispersity index obtained in DLS was always higher than 0.15 indicating a relatively broad distribution of the particle size, also confirmed by the shape of UV-Vis analysis. This broad size distribution is partly a consequence of the velocity profiles under laminar flow regime. Figure 5 and Table 2 show the analysis of size distribution obtained from TEM images, for microwaves and conventional heating at the different flow rates. The software ImageJ was adopted to determine the size distribution. A clear correlation of residence time and size of the particles is observed. For both of systems, an increase in flow rate shifts the size distribution to lower diameter values. Moreover, the particle diameter is dependent on the heating source. Particles synthesized by microwaves are almost twice as big as particles obtained by CH indicating a more intense reaction under MWH. On the other hand, size distribution was broader for conventional heating, as indicated by the relative standard deviation in Table 2, which is roughly double when comparing CH vs. MWH. Less pronounced difference was observed by Hongjin Jiang³⁴, who noticed a shift of relative standard from 0.46 to 0.36 respectively for CH and MWs.

Ag synthesized NPs were highly crystalline, as it inferred from HRTEM images of two representative nanoparticles (Figure 6). Fourier transform analysis revealed a face-centered cubic symmetry, characteristic of the Ag packing in NPs with Fm3m crystallographic space group (Figure 6).

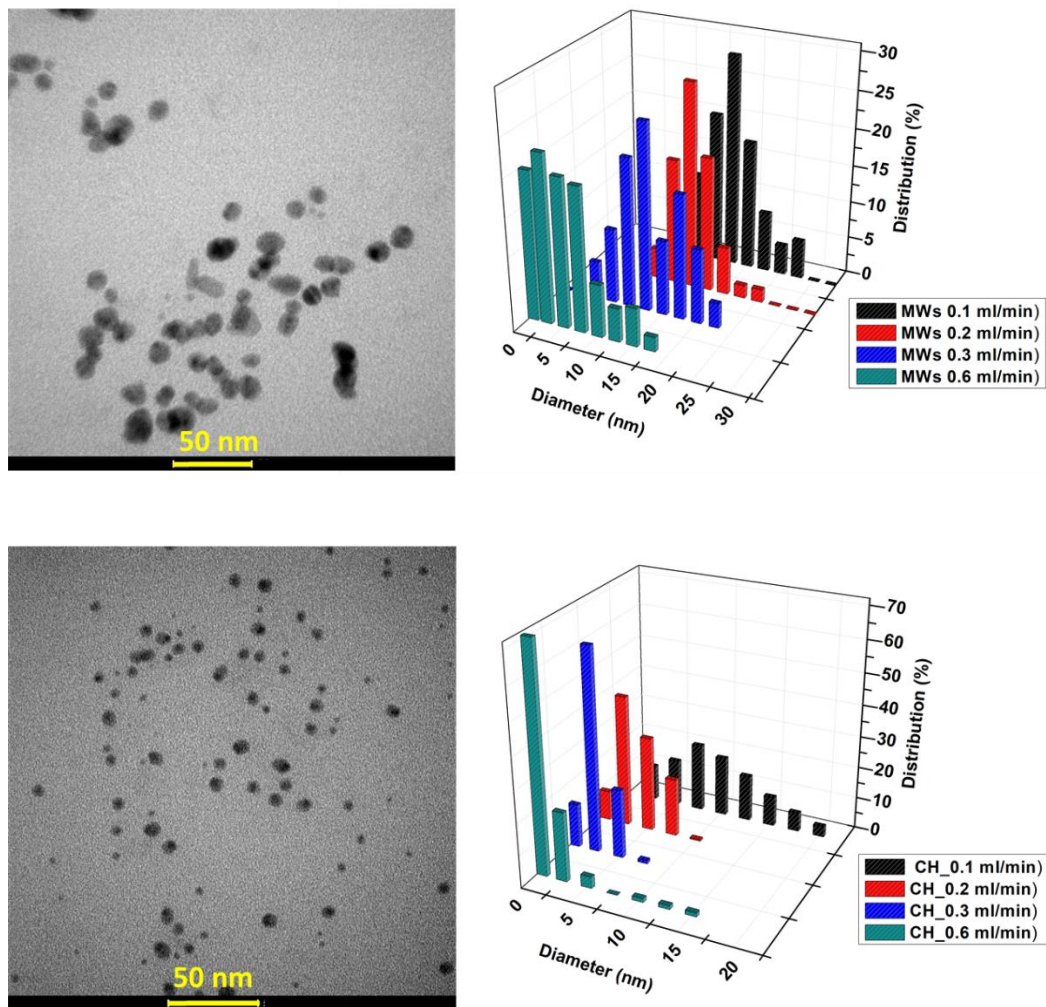


Figure 5 Particle size distribution at different flow rates and representative TEM images for a flow rate of 0.2 ml/min, scale bar 50 nm.

Table 2: TEM analysis distribution for Microwaves and Conventional Heating. N stands for the number of nanoparticles measured to obtain the nanoparticles size distribution histogram.

\dot{V} (ml/min)	TEM Analysis					
	MWH			CH		
	Mean Value (nm)	Rel. Stan. Dev.	N meas.	Mean Value (nm)	Rel. Stan. Dev.	N meas.
0.1	19.0±4.3	0.23	226	10.8±4.7	0.44	269
0.2	14.3±2.9	0.20	182	5.1±2.1	0.41	233
0.3	14.0±4.3	0.31	185	3.8±1.7	0.45	121
0.6	5.8±3.4	0.59	195	2.7±2.4	0.88	128

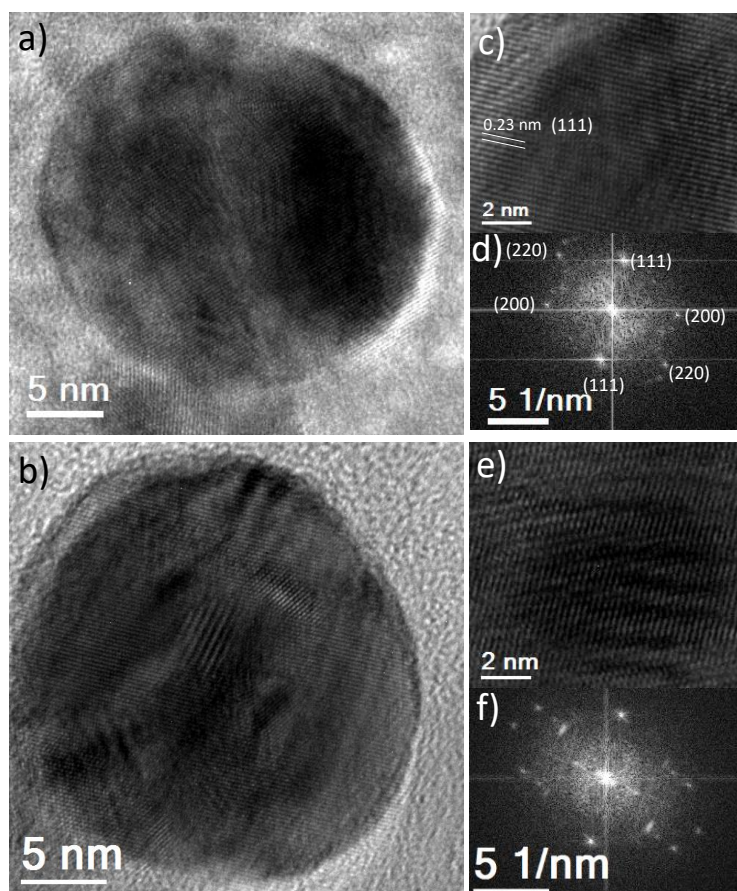
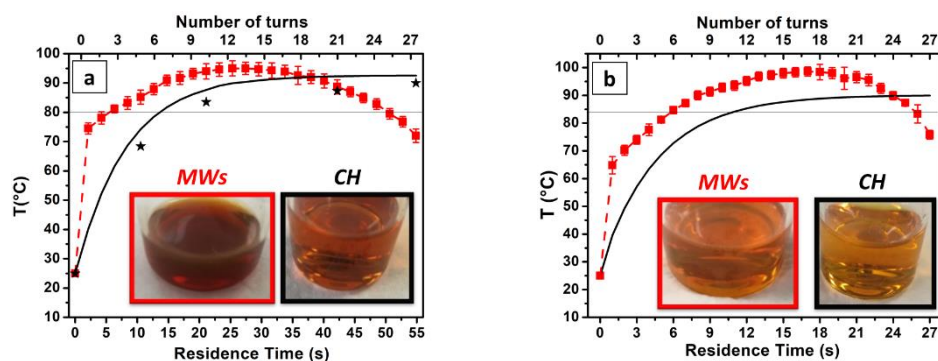


Figure 6 a)-b) High-resolution TEM analysis of AgNPs produced by MWH, flow rate 0,1ml/min. c-e) Micrographs showing fine detail of a single AgNP; d)-f) Fourier function transform (FFT) analysis of a) and b); where crystal planes and d-spacing corresponds to Fm3m space group.

Temperature profile evaluation

A detailed evaluation of the temperature profile was performed to justify the differences in synthesis yield and size distribution obtained with the two heating systems. A slow nucleation mechanism may occur even at room temperature between the Y-mixer and the heating zone (lpipe=8cm, as reported in figure S1). However, considering the small volume of the concerned section of the reactor (nominal residence times in that zone would be at least 5.6 seconds) and the slow kinetics for this low temperature the extent of particles nucleation before the heating step can be neglected in this work. For MWH, a preliminary study allowed to compare data of IR camera, recording the wall temperature of the Teflon pipe, and the readings of the O.F. inserted inside the tubing. The temperature recorded with the IR camera in the last turn was very close to the temperature recorded with the O.F. (position O.F.1 of Figure 2), with a difference always lower than 2°C. This confirmed that the temperature drops along the thickness of the Teflon tube (0.6mm) is negligible and the IR camera temperature is a good approximation of the internal flow

temperature. Thus, the temperature profile along the tube could be determined by calculating the average temperature of the area of each pipe turn, recorded by thermographs of IR camera. In the case of conventional heating, the internal flow temperature was simulated by COMSOL Multiphysics, as described in the experimental section. Figure 6 presents the temperature profiles for the 4 different residence times studied, in red for thermographic camera measurements in MWH and in black simulation for CH. The black star symbols correspond to the experimental measurement of the optical fiber in CH at 4 different points (5, 10, 20 and 25 turns), measured for a flow rate of 0.1 ml/min. The experimental values agree well with the simulated line, validating the model parameters and the calculated heat transfer coefficient for CH. Looking at the two temperature profiles, it is clear that the temperature reached by the fluid under CH is always lower compared to the fluid heated by MW. This is mainly due to the strong reduction of heating length achieved under MWH conditions, where reaction temperature is approached much faster, as shown in figure 7 under any of the conditions employed. This observation correlates with the lower synthesis yield achieved in CH and explains the differences observed in terms of nanoparticle size and concentration, in agreement with previous analysis suggesting that thermal effects are responsible for the higher synthesis yield obtained by microwave heating³⁵. In the case of the lowest flow 0.1 ml/min the temperature of the fluid is above 75°C for 95% of the length of the reactor, however this is only true for around 80%, in the case of CH, leading to a lower synthesis yield. As flow rate increased, the differences in the temperature profile are less pronounced which also explains that the UV-VIS spectra intensity is more similar in both heating rates for the cases of 0.3 and 0.6 ml/min although a more intense reaction is always observed for MWH.



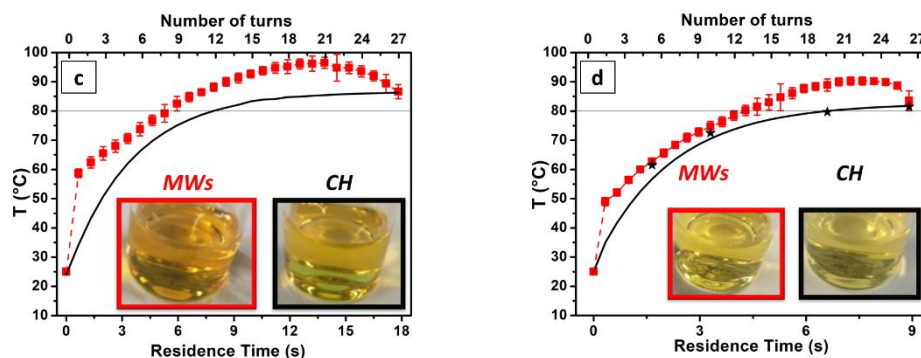


Figure 7: Temperature profiles for 20W-MWs (red color-experimental values) and CH (black color line –simulated data, black stars –experimental values) at different flow rates:

a-0.1ml/min, b-0.2ml/min, c-0.3ml/min and d-0.6ml/min.

Finally, the measurement of the temperature in the position O.F.2 of Figure 2 demonstrated the fast cooling: from a temperature higher than 80°C at the end of the reactor, the fluid temperature dropped to 30°C immediately outside of the cavity. This fast decrease of temperature helped to quench the reaction preventing further uncontrolled growth (as confirmed by the narrower particle size distribution), and also increased rapidly fluid viscosity, hindering the subsequent aggregation of the nanoparticles.

Deposition of nanoparticles on the wall

Another advantage of using microwaves was the strong decrease of wall deposition (see Figure 8 and table S1 in supplementary information). This could be directly observed thanks to the transparent reactor wall used. Thus for instance, in the case of the highest residence time used the deposition of nanoparticles on the wall of reactor under CH is evident and contrasts to the almost clear surface observed for the MWH heated system. Only in the case of 0.6ml/min the wall was completely clean under CH. To quantitative analyze the difference of silver deposition, the portion of the Teflon pipe showing higher fouling was analyzed by SEM for the samples MWs_0.1ml/min and CH_0.1ml/min, where we have the maximum contact time between particles and reactor wall. The longitudinal section analyzed confirmed the first visual impression (figure 6), a much higher concentration of silver was observed for the conventional heating. In detail, the deposition value, defined as the ratio of the silver concentration to Teflon pipe surface, shifted from 18% of CH to 3% for MWs, determined from the quantitative color contrast of SEM images by the software ImageJ. The observed wall fouling agreed well with the temperature profile simulations under CH conditions since no deposition was observed in the first seven turns, where the temperature was lower than 80°C, as reported in figure 6a). The high constant temperature, observed in the second portion of the reactor, increased both the subsequent aggregation of the particles and the wetting of the Teflon surface, resulting in a higher wall deposition. Furthermore, there is a strict correlation

between the wall deposition and the particles size distribution observed. As the growth occurs through an autocatalytic process, the particles concentration decreases leading to a lower growth rate. These effects were drastically reduced by the parabolic temperature profile observed for MWH.

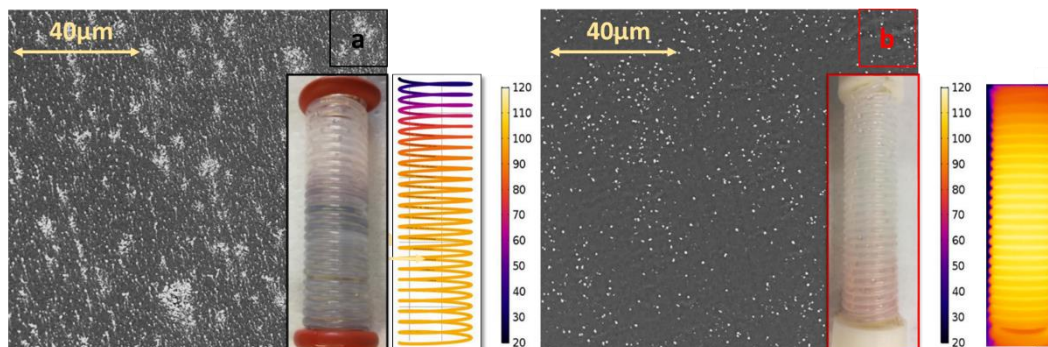


Figure 8. HR-SEM pictures showing representative views of the areas of the reactor wall with the highest fouling under MWH (right) and CH (left) for a flow rate of 0.1ml/min. For CH the COMSOL simulation of temperature profile is also presented on the CH figure, while IR thermograph of the reactor is shown for MWH.

4. CONCLUSIONS

Microfluidic synthesis of silver nanoparticles allows the continuous production of small unaggregated silver nanoparticles with tunable particle sizes. Comparing the different results obtained by UV-Vis, MS-AES, DLS and TEM, the syntheses of Ag NPs obtained under MWH demonstrated a faster heating rate and a more extensive growing rate than the CH. Furthermore, the fast decrease of temperature, that characterized MWH, allowed to better control particle size growth, reducing the relative standard deviation of size distribution. Moreover, a considerable reduction of the wall deposition was observed with MWH. For this reason, the combination of microfluidic processing and homogeneous MWH may represent an ideal system for the synthesis of silver nanoparticles. The polydispersity still observed is a consequence of laminar velocity profiles and could be reduced by transition to plug flow behavior using segmented flow. However, for the sake of simplicity this aspect has not been explored as this work has focused on the comparison of MWH and CH for the same reaction conditions. The differences in temperature distribution for CH and MWH systems reflect the different heating patterns responsible for the higher reaction yields and lower wall fouling observed. Finally, the faster cooling achieved under MWH reduced the possibility of agglomeration of the nanoparticles and helped to narrow the particle size distribution.

ASSOCIATED CONTENT

Supporting Information

Experimental Microfluidic Reactor (Figure S1). Parameters and details of COMSOL simulation (Table S1 and Table S2). Map of the inner flow (Table S3) and Mesh Size Element Dependence (Table S4). TEM images (Table S5), DLS size distribution (Figure S2) and reactor wall deposition (Table S7) at different flow rates for Conventional Heating and Microwave Heating. Nomenclature of symbols.

Author information

(*) Institute of Nanoscience of Aragon (INA) and Department of Chemical Engineering and Environmental Technology, University of Zaragoza, C/Mariano Esquillor, s/n, I+D+i Building, 50018, Zaragoza, Spain. Email: rmallada@unizar.es ; Email: victorse@unizar.es ; Fax: +34 976 761879 ; Tel: +34 876555441

Acknowledgments

This project has received funding from the European Union's Horizon 2020 research and innovation programme under the Marie Skłodowska-Curie grant agreement No 721290. This publication reflects only the author's view, exempting the Community from any liability. Project website: <http://cosmic-etn.eu/>.

Financial support from CIBERBBN (initiative funded by the VI National R&D&i Plan 2008–2011, Iniciativa Ingenio 2010, Consolider Program, CIBER Actions and financed by the Instituto de Salud Carlos III with assistance from the European Regional Development Fund) is gratefully acknowledged.

The microscopy works have been conducted in the Laboratorio de Microscopias Avanzadas at Instituto de Nanociencia de Aragón—Universidad de Zaragoza. Authors acknowledge the LMA-INA for offering access to their instruments and expertise.

References

- (1) Afzal, A.; Kim, K. Y. Convergent-Divergent Micromixer Coupled with Pulsatile Flow. *Sensors Actuators, B Chem.* **2015**, *211*, 198.
- (2) Lee, C. Y.; Chang, C. L.; Wang, Y. N.; Fu, L. M. Microfluidic Mixing: A Review. *Int. J. Mol. Sci.* **2011**, *12*, 3263.
- (3) The, H. Le; Ta, B. Q.; Thanh, H. Le; Dong, T.; Thoi, T. N.; Karlsen, F. Geometric Effects on Mixing Performance in a Novel Passive Micromixer with Trapezoidal-Zigzag Channels. *J. Micromechanics Microengineering* **2015**, *25*, 094004.
- (4) Wagner, J.; Köhler, J. M. Continuous Synthesis of Gold Nanoparticles in a Microreactor. *Nano Lett.* **2005**, *5*, 685.
- (5) Helmlinger, J.; Heise, M.; Heggen, M.; Ruck, M.; Epple, M. A Rapid, High-Yield and Large-Scale Synthesis of Uniform Spherical Silver Nanoparticles by a Microwave-Assisted Polyol Process. *RSC Adv.* **2015**, *5*, 92144.
- (6) Zhao, C. X.; He, L.; Qiao, S. Z.; Middelberg, A. P. J. Nanoparticle Synthesis in Microreactors. *Chem. Eng. Sci.* **2011**, *66*, 1463.
- (7) Martínez, G.; Sebastián, V.; Hueso, J. L. Alternative Methodologies for the Production of Nanomaterials Based on Microfluidics and Laser Pyrolysis Technologies. *Manuf. Nanostructures* **2015**, 417.
- (8) Sebastián, V.; Jensen, K. F. Nanoengineering a Library of Metallic Nanostructures Using a Single Microfluidic Reactor. *Nanoscale* **2016**, *8*, 15288.
- (9) Makgwane, P. R.; Ray, S. S. Synthesis of Nanomaterials by Continuous-Flow Microfluidics: A Review. *J. Nanosci. Nanotechnol.* **2014**, *14*, 1338.
- (10) Ma, J.; Lee, S. M.; Yi, C.; Li, C. Controllable Synthesis of Functional Nanoparticles by Microfluidic Platforms for Biomedical Applications – a Review. *Lab Chip* **2017**, No. 17, 209.
- (11) Lu, M.; Ozcelik, A.; Grigsby, C. L.; Zhao, Y.; Guo, F.; Leong, K. W.; Tony. Microfluidic Hydrodynamic Focusing for Synthesis of Nanomaterials. *HHS Public Access* **2016**, *11*, 778.
- (12) Song, Y.; Hormes, J.; Kumar, C. S. S. R. Microfluidic Synthesis of Nanomaterials. *Small* **2008**, *4*, 698.
- (13) Chandrasekaran, S.; Ramanathan, S.; Basak, T. Microwave Material Processing—a Review. *AIChE J.* **2012**, *58*, 330.
- (14) Saxena, V. K. K.; Chandra, U.; Chandr, U. Microwave Synthesis: A Physical Concept. *Microw. Heat.* **2011**, No. April, 3.
- (15) Tsuji, M.; Hashimoto, M.; Nishizawa, Y.; Kubokawa, M.; Tsuji, T. Microwave-Assisted Synthesis of Metallic Nanostructures in Solution. *Chem. - A Eur. J.* **2005**, *11*, 440.
- (16) Gawande, M. B.; Shelke, S. N.; Zboril, R.; Varma, R. S. Microwave-Assisted Chemistry: Synthetic Applications for Rapid Assembly of Nanomaterials and Organics. *Acc. Chem. Res.* **2014**, *47*, 1338.
- (17) Gerbec, J. A.; Magana, D.; Washington, A.; Strouse, G. F. Microwave-Enhanced Reaction Rates for Nanoparticle Synthesis. *J. Am. Chem. Soc.* **2005**, *127*, 15791.
- (18) Horikoshi, S.; Serpone, N. *Microwaves in Catalysis. Methodology and Applications.*; Wiley Online Library, 2015.

- (19) Gjuraj, E.; Kongoli, R.; Shore, G. Combination of Flow Reactors with Microwave-Assisted Synthesis: Smart Engineering Concept for Steering Synthetic Chemistry on the “Fast Lane.” *Chem. Biochem. Eng. Q.* **2012**, *26*, 285.
- (20) Horikoshi, S.; Sumi, T.; Serpone, N. A Hybrid Microreactor/Microwave High-Pressure Flow System of a Novel Concept Design and Its Application to the Synthesis of Silver Nanoparticles. *Chem. Eng. Process. Process Intensif.* **2013**, *73*, 59.
- (21) Glasnov, T. N.; Kappe, C. O. Microwave-Assisted Synthesis under Continuous-Flow Conditions. *Macromol. Rapid Commun.* **2007**, *28*, 395.
- (22) Horikoshi, S.; Abe, H.; Torigoe, K.; Abe, M.; Serpone, N. Access to Small Size Distributions of Nanoparticles by Microwave-Assisted Synthesis. Formation of Ag Nanoparticles in Aqueous Carboxymethylcellulose Solutions in Batch and Continuous-Flow Reactors. *Nanoscale* **2010**, *2*, 1441.
- (23) Nishioka, M.; Miyakawa, M.; Kataoka, H.; Koda, H.; Sato, K.; Suzuki, T. M. Continuous Synthesis of Monodispersed Silver Nanoparticles Using a Homogeneous Heating Microwave Reactor System. *Nanoscale* **2011**, *3*, 2621.
- (24) Liu, Q.; Gao, M. R.; Liu, Y.; Okasinski, J. S.; Ren, Y.; Sun, Y. Quantifying the Nucleation and Growth Kinetics of Microwave Nanochemistry Enabled by in Situ High-Energy X-Ray Scattering. *Nano Lett.* **2016**, *16*, 715.
- (25) Özkar, S.; Finke, R. G. Silver Nanoparticles Synthesized by Microwave Heating: A Kinetic and Mechanistic Re-Analysis and Re-Interpretation. *J. Phys. Chem. C* **2017**, *121*, 27643.
- (26) Dzido, G.; Markowski, P.; Małachowska-Jutysz, A.; Prusik, K.; Jarzębski, A. B. Rapid Continuous Microwave-Assisted Synthesis of Silver Nanoparticles to Achieve Very High Productivity and Full Yield: From Mechanistic Study to Optimal Fabrication Strategy. *J. Nanoparticle Res.* **2015**, *17*, 26.
- (27) Khodashenas, B.; Ghorbani, H. R. Synthesis of Silver Nanoparticles with Different Shapes. *Arab. J. Chem.* **2014**, No. **12**, 1878.
- (28) Nigar, H.; Julián, I.; Mallada, R.; Santamaría, J. Microwave-Assisted Catalytic Combustion for the Efficient Continuous Cleaning of VOC-Containing Air Streams. *Environ. Sci. Technol.* **2018**, *52*, 5892.
- (29) Nigar, H.; Sturm, G. S. J.; Mallada, R.; Stankiewicz, A.; Santamaría, J. Numerical Analysis of Microwave Heating Cavity: Combining Electromagnetic Energy, Heat Transfer and Fluid Dynamics for a NaY Zeolite Fixed-Bed. *Appl. Therm. Eng.* **2019**, *155*, 226.
- (30) Prasad, B.; Shaban, M. K.; Haneef, S.; Raj, V. Comparison of Heat Transfer between a Helical and Straight Tube Heat Exchanger. *Int. J. Eng. Res. Technol.* **2013**, *6*, 974.
- (31) Mulvaney, P. Surface Plasmon Spectroscopy of Nanosized Metal Particles. *Langmuir* **1996**, No. 12, 788.
- (32) Baber, R.; Mazzei, L.; Thanh, T. K.; Gavriilidis, A. Synthesis of Silver Nanoparticles in a Micro Fluidic Coaxial Flow Reactor. *RSC Adv.* **2015**, No. **5**, 95585.
- (33) Slistan-Grijalva, A.; Herrera-Ubina, R.; Silva-Rivas, J. F.; Ávalos-Borja, M.; Castellón-Barraza, F. F.; Posada-Amarillas, A. Classical Theoretical Characterization of the Surface Plasmon Absorption Band for Silver Spherical Nanoparticles Suspended in Water and Ethylene Glycol. *Physica* **2015**, *27*, 104.
- (34) Jiang, H.; Moon, K.; Zhang, Z.; Pothukuchi, S.; Wong, C. P. Variable Frequency

- Microwave Synthesis of Silver Nanoparticles. *J. Nanoparticle Res.* **2006**, *8*, 117.
- (35) Baghbanzadeh, M.; Carbone, L.; Cozzoli, P. D.; Kappe, C. O. Microwave-Assisted Synthesis of Colloidal Inorganic Nanocrystals. *Angew. Chemie - Int. Ed.* **2011**, *50*, 11312.

For Table of Contents Only

